Oscillatory dynamics in a heterogeneous surface reaction: Breakdown of the mean-field approximation

R. Dennis Vigil* and Frank T. Willmore†
Department of Chemical Engineering, Iowa State University, Ames, Iowa 50011-2230
(Received 1 April 1996)

Hierarchical mean-field rate equations and lattice-gas simulations were developed to elucidate the effects of the breakdown of the mean-field approximation for a model heterogeneous chemical oscillator that represents a simple extension of the well-known monomer-dimer surface reaction model. The bifurcation structure of the reaction kinetics depends sensitively on the details of surface transport processes, and the oscillatory behavior exhibited by the site approximation rate equations is not generally robust with respect to spatial correlations. [S1063-651X(96)07308-4]

PACS number(s): 05.40.+j, 82.20.Mj, 82.40.−g

INTRODUCTION

Surface reaction schemes with elementary steps involving neighboring pairs of adsorption sites and adsorbates (e.g., dissociative adsorption) can be exactly represented only by an infinite hierarchy of coupled rate equations that describe progressively larger configurations of reactants [1–3]. The traditional approach to overcoming this closure problem is to invoke the mean-field site approximation (SA), which requires that the probability of finding a given adsorption site in a particular occupation state be independent of the occupation states of neighboring sites. This condition implies that transport processes are sufficiently rapid so that the surface is microscopically well mixed. However, such an assumption is not always warranted, as in the case of CO oxidation, where oxygen can be strongly bound to the surface [4].

During the past decade, the effects of the breakdown of the SA on the bifurcation structure of catalytic surface reactions have attracted considerable attention. Most of this work has been directed toward the monomer-dimer model, which mimics some aspects of CO oxidation. The scheme consists of the Langmuir-Hinshelwood mechanism

$$A + V \overset{1}{\leftrightarrow} A(\mathrm{ad}), \tag{1a}$$

$$B_2 + 2V \overset{2}{\rightarrow} 2B(\mathrm{ad}), \tag{1b}$$

$$A(\mathrm{ad}) + B(\mathrm{ad}) \overset{3}{\rightarrow} AB + 2V, \tag{1c}$$

where V represents a vacant adsorption site and processes (1b) and (1c) are implicitly assumed to occur at nearest-neighbor pairs of sites. The non-mean-field behavior of this reaction was explored by Ziff, Gulari, and Barshad, who introduced a stochastic lattice-gas implementation of the model (the ZGB model) with an infinite reaction rate ($k_3=\infty$) and irreversible monomer adsorption ($k_{-1}=0$) [5]. Their results showed that spatial correlations can have significant effects on the structure of the reaction kinetics. For example, the SA equations corresponding to the ZGB model predict reaction-adsorption isotherms that display bistability between a reactive and an A-poisoned state [6]. In contrast, the ZGB model predicts a first-order A-poisoning transition with associated metastability as well as a second-order B-poisoning transition [5]. Such discrepancies between SA and lattice-gas predictions have inspired efforts to model the behavior of surfaces with intermediate degrees of mixing and to develop a unified treatment of surface reaction kinetics [4,6–11]. However, little is known about the breakdown of the SA for reaction schemes with more complicated dynamics than the monomer-dimer model, which exhibits only fixed-point behavior and bistability. The purpose of this paper is to delineate some effects of spatial correlations on an oscillatory surface reaction model by comparing the predictions of mean-field rate equations and lattice-gas simulations.

MODEL

Although the monomer-dimer model (1a)–(1c) does not support periodic behavior, it can be modified in one of several ways so that it does predict oscillatory solutions. These include allowing the reaction product to desorb at a finite rate [12], relaxing the isothermal assumption [13], or adding a reversibly adsorbing inert species [14]. In this work we consider the latter model by adding the reversible adsorption step

$$C + V \overset{4}{\leftrightarrow} C(\mathrm{ad}) \tag{1d}$$

to the reaction mechanism (1a)–(1c).

MEAN-FIELD SITE APPROXIMATION

A simple site approximation representation of processes (1a)–(1d) can be developed by invoking the following assumptions: isothermal conditions, instantaneous product desorption, no mass transfer resistance between the fluid and catalyst, energetically homogeneous adsorption sites, no ad-

*Author to whom correspondence should be addressed.
†Present address: Department of Chemical Engineering, University of Texas, Austin, TX 78712.

TABLE I. Dimensionless parameters. The quantity p_i represents the gas phase partial pressure of species i.

$$\alpha = \frac{k_1 p_A}{k_3 S_0}$$
$$\gamma = \frac{k_{-1}}{k_3 S_0}$$
$$\beta = \frac{k_2 p_{B_2}}{k_3}$$
$$\lambda = \frac{k_4 p_C}{k_3 S_0}$$
$$\eta = \frac{k_{-4}}{k_3 S_0}$$

sorbate interactions beyond site exclusion, and constant gas phase composition and volume. On a square lattice of adsorption sites, the resulting dimensionless rate equations are given by

$$\frac{d\theta_A}{d\tau} = \alpha\theta_V - \gamma\theta_A - 4\theta_A\theta_B, \tag{2a}$$

$$\frac{d\theta_B}{d\tau} = 2\beta\theta_V^2 - 4\theta_A\theta_B, \tag{2b}$$

$$\frac{d\theta_C}{d\tau} = \lambda\theta_V - \eta\theta_C, \tag{2c}$$

where θ_i is the fraction of adsorption sites occupied by species i and the vacant site fraction obeys $\theta_V = 1 - \theta_A - \theta_B - \theta_C$. If the total density of adsorption sites is S_0, the dimensionless time is given by $\tau = k_3 S_0 t$ and five dimensionless parameters are related to the adsorption and reaction rate constants, as shown in Table I. Notice that both γ and η depend primarily on the reaction and desorption rate coefficients, which are generally functions of temperature. Therefore, from a practical standpoint, it is not possible to manipulate the value of either of these parameters without simultaneously causing all other parameters to change as well, since every dimensionless parameter depends upon the reaction rate constant. In contrast, α, β, and λ are additionally proportional to concentrations of gas phase species, which in principle can be varied independently. Therefore, for fixed temperature, only α, β, and λ are appropriate bifurcation parameters.

As a consequence of the assumption that B_2 adsorbs irreversibly, Eq. (2b) dictates that the adsorbed dimer can be removed from the surface only by reaction. This leads to the existence of a trivial B-poisoned state $\theta_B = 1, \theta_A = \theta_C = 0$. Analogous A- or C-poisoned states do not exist since adsorption of these species is taken to be reversible. Nontrivial steady-state solutions θ_i can readily be found from Eqs. (2a)–(2c) and are given implicitly by

$$\overline{\theta_B^3} + \left[\frac{\alpha}{2\beta\eta}(\lambda+\eta) + 2\gamma - 1\right]\overline{\theta_B^2} + \left[\frac{\alpha\gamma}{2\beta\eta}(\lambda+\eta) + \gamma(\gamma-2) + \frac{\alpha^2}{2\beta}\right]\overline{\theta_B} - \gamma^2 = 0, \tag{3a}$$

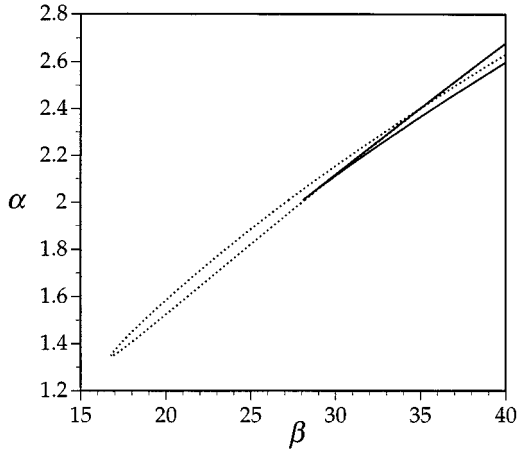

FIG. 1. Bifurcation diagram in α-β parameter space. Solid lines represent the locus of saddle nodes, terminating in a cusp. Dotted lines represent Hopf points, which terminate at double-zero eigenvalue bifurcations (not shown). Other parameters values used to construct the figure are $\gamma = 0.04$, $\lambda = 0.36$, and $\eta = 0.016$.

$$\overline{\theta_A} = \frac{\alpha\eta(1-\overline{\theta_B})}{(\overline{\theta_B}+\gamma)(\lambda+\eta)+\alpha\eta}, \tag{3b}$$

$$\overline{\theta_C} = \frac{\lambda(1-\overline{\theta_A}-\overline{\theta_B})}{\lambda+\eta}. \tag{3c}$$

Note that in the limit $\beta \to \infty$, Eq. (3a) has a single real positive root that approaches the B-poisoned state $\theta_B = 1$. Except in this asymptotic limit, the poisoned state is locally unstable and therefore it will not be considered further. For finite values of β, Eq. (3a) has either one or three real positive roots and some conditions exist for which a cusp bifurcation occurs.

The bifurcation structure of Eqs. (2a)–(2c) can be studied with continuation techniques. The software package AUTO developed by Doedel and Wang [15] was employed for this purpose, and the reliability of the calculations was verified by direct numerical integration of Eqs. (2a)–(2c). Figure 1 shows a typical bifurcation diagram in α-β parameter space. The cusp and loop structures are common features of both homogeneous and heterogeneous chemical oscillators. Fixed-point bistability boundaries (solid lines) are formed by a locus of saddle-node bifurcation points that terminate in a cusp. Hopf points form a loop (broken lines) that ends at degenerate double-zero eigenvalue bifurcations on each saddle-node branch. The Hopf and saddle-node points divide parameter space into several regions (some of which are very small) with qualitatively distinct reaction-adsorption isotherms, and some of these regions can be subdivided further by plotting the locus of limit cycle branch saddle nodes.

MEAN-FIELD PAIR APPROXIMATION

A higher-order truncation of the hierarchical rate equations can be derived by considering the occupancy of neighboring *pairs* of sites, which are assumed to be randomly distributed on the surface. The resulting mean-field model is

known as a pair approximation (PA) [1–3] and it accounts for nearest-neighbor spatial correlations in the distribution of reactants. One defines N_{ij} to be the number of pairs of sites occupied by species i and j. Since a square lattice of N sites with periodic boundaries has $2N$ nearest-neighbor pairs, the fractional pair coverages are defined as $X_{ij}=N_{ij}/2N$. Conservation equations for the X_{ij} can be constructed by calculating the rate of change of each pair type for each elementary step of the mechanism. For example, dimer adsorption (1b) occurs at a rate $k_2 X_{VV}$ and can be represented schematically as

$$\begin{array}{ccccc} & X & X & & \\ X & V & V & X & \end{array} \xrightarrow{k_2} \begin{array}{ccccc} & X & X & & \\ X & B & B & X & \end{array},$$

where X represents a site that can be in any occupation state. Nearest-neighbor pairs that are potentially affected by this process include AV, BV, CV, VV, AB, BB, and BC. In order to calculate changes in the pair coverages, one must know the conditional probability $P(j|i)$ of finding a neighboring site in occupation state j given a site in occupation state i. For a square lattice these probabilities are given by [1]

$$P(j|i)=\begin{cases} \dfrac{X_{ij}}{2\theta_i}, & i\neq j \\ \dfrac{X_{ij}}{\theta_i}, & i=j \end{cases} \tag{4}$$

and the changes in pair coverage fractions follow easily from Eq. (4). For example, B_2 adsorption can result in the loss of at most six AV pairs, so we write

$$\left.\frac{dX_{AV}}{dt}\right|_{(1b)} = \frac{1}{2N}\frac{dN_{AV}}{dt} = -\frac{3k_2 X_{VV} X_{AV}}{2\theta_V}, \tag{5}$$

where $\theta_i = X_{ii} + \frac{1}{2}\Sigma_{i\neq j} X_{ij}$. Proceeding in this way for each elementary step of the reaction, dimensionless rate equations for the evolution of the coverage of ten possible pair types can be derived.

The intermediate behavior between the pair and site approximations can be studied by incorporating surface transport processes into the PA. For example, one can allow the hopping process

$$\begin{array}{ccccc} & X & X & & \\ X & Y & V & X & \end{array} \xrightarrow{d_Y} \begin{array}{ccccc} & X & X & & \\ X & V & Y & X & \end{array},$$

where Y represents an adspecies. Complete dimensionless PA equations that include terms to account for adsorbate hopping are given in the Appendix. From these, it can be shown that as $d_i \to \infty$, spatial fluctuations are destroyed, the pair fractions are given by

$$X_{ij}=\begin{cases} 2\theta_i\theta_j, & i\neq j \\ \theta_i^2, & i=j, \end{cases} \tag{6}$$

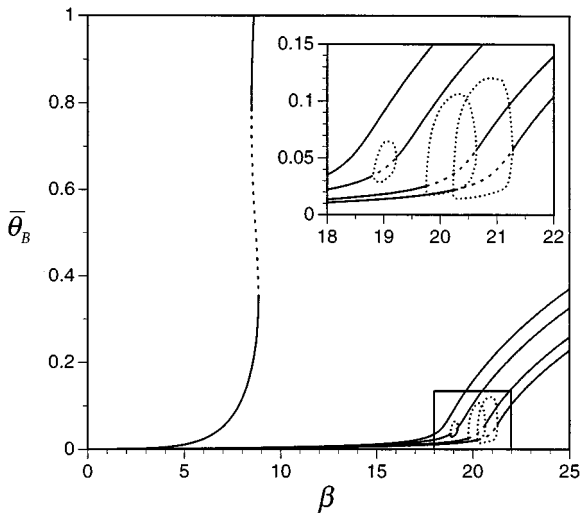

FIG. 2. Reaction-adsorption isotherms showing the convergence of the pair approximation and site approximation at high hop rates when all adspecies have identical hopping rate constants. The curves from left to right represent the pair approximation with $d_i/k_3=0,1,10,50$. The last curve shows the SA prediction. Solid lines represent stable fixed-point solutions, dashed lines represent unstable fixed points, and dotted lines show maxima and minima of stable limit cycle solutions. Other parameter values used to construct the figure are $\alpha=1.6$, $\gamma=0.04$, $\lambda=0.36$, and $\eta=0.016$.

and the site approximation is recovered from the pair equations.

Computations using the PA equations described above show that nearest-neighbor correlations can destroy the oscillatory structures predicted by the SA. For example, Fig.2 shows reaction-adsorption isotherms calculated from the SA and the PA for the case that all adspecies have identical hopping constants ($d_A=d_B=d_C$). When no adsorbate hopping is allowed, the PA predicts only fixed-point solutions. However, as the hopping constants are increased, the PA predictions converge to the SA and oscillatory solutions are recovered. For the parameters used to construct Fig. 2, oscillatory behavior was found for approximately $d_i/k_3>10$. Notice that the pure pair approximation ($d_i=0$) predicts a small region of bistability between a reactive and a B-poisoned state. The existence of a discontinuous dimer poisoning transition in this model contrasts with the PA predictions for the simpler monomer-dimer model, which exhibits a second-order dimer poisoning transition.

The PA predictions for the more general case of unequal hopping rates have also been considered. For example, Fig. 3 shows reaction-adsorption isotherms for the three cases in which only one adspecies is mobile; all other parameter values are the same as in Fig. 2. Notice that the pair equations fail to predict oscillatory structures for all of these situations, regardless of how large the hopping rate of the mobile adspecies becomes. Furthermore, the structure of the reaction-adsorption isotherms depends upon which species is taken to be mobile. For example, when the monomer A is the hopping species, a region of bistability exists for all values of d_A and dimer poisoning occurs at a finite value of β, the dimensionless partial pressure of B_2. In contrast, when the dissociated

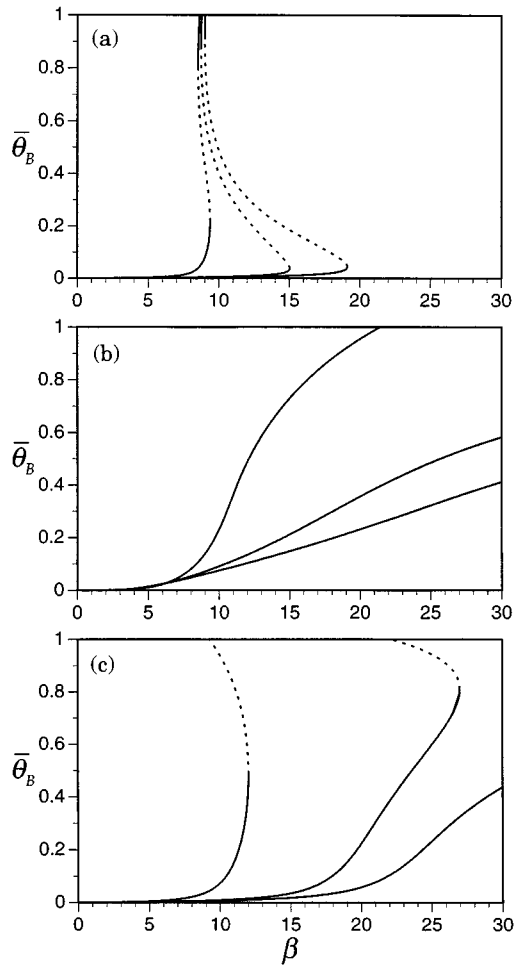

FIG. 3. Pair approximation predictions for the case in which only one adspecies is mobile. The adsorbed monomer is mobile in (a), the dimer is mobile in (b), and the inert is mobile in (c). The three curves in each plot from left to right represent reaction-adsorption isotherms for $d_i/k_3=1,10,100$, respectively. Larger values of the dimensionless hopping constants do not give significantly different results. Other parameters are the same as those used to construct Fig. 2.

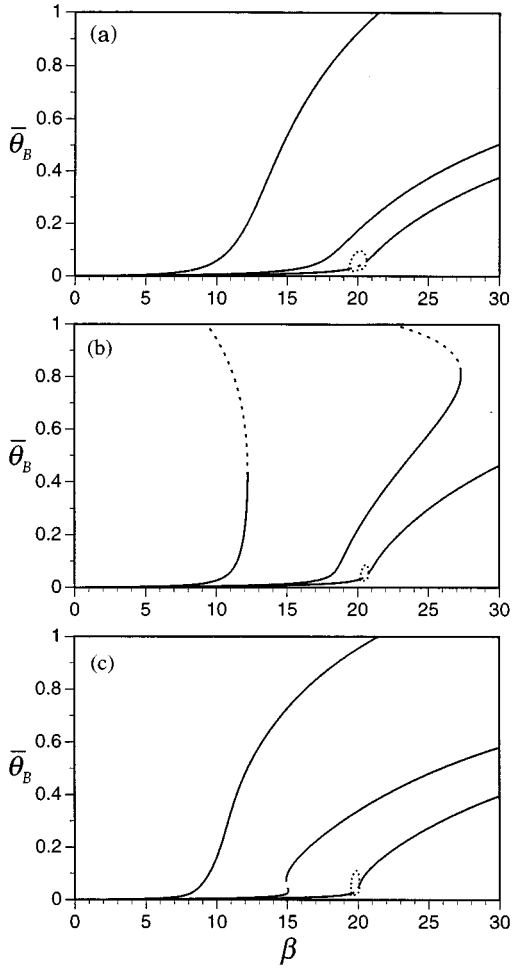

FIG. 4. Pair approximation predictions for the case in which only one adspecies is immobile and the hopping constants of the other two species are identical. The adsorbed monomer is immobile in (a), the dimer is immobile in (b), and the inert is immobile in (c). The three curves in each plot from left to right represent reaction-adsorption isotherms for $d_i/k_3=1,10,100$, respectively. Other parameters are the same as those used to construct Fig. 2.

dimer B is taken as the mobile species, multiple steady states do not exist except when the hopping rate constant d_B is nearly zero.

Different results are obtained when it is assumed that only one species is immobile while the other two species have identical hopping rate constants. The results for the three possible combinations are illustrated in Fig. 4. In all three cases, the oscillatory dynamics predicted by the SA can be recovered by sufficiently increasing the value of the hopping rate constants. However, again the character of the reaction-adsorption isotherms depends upon which species is taken to be immobile. As an example, consider the scenario where the inert monomer C is immobile. Figure 4(c) shows that when $d_A/k_3=d_B/k_3=1$, a unique steady state exists for all β. Since the pair equations with no surface hopping predict a narrow region of bistability (Fig. 2), it appears that increasing these two dimensionless hop rate constants from zero to 1 leads to an unfolding of the bistability loop. However, after further increasing $d_A/k_3=d_B/k_3=10$, a hysteresis loop appears. Subsequent increases in d_A and d_B again unfold the hysteresis loop and the limit cycle behavior predicted by the SA emerges. In contrast, bistability is not observed in Fig. 4(a) for any of the dimensionless hop rate constants considered.

LATTICE-GAS SIMULATIONS

In principle, higher-order truncations of the hierarchical rate equations, such as the triplet approximation, can also be developed. In practice, however, the resulting sets of equations are too unwieldy. Therefore, a stochastic lattice-gas implementation of processes (1a)–(1d) was employed.

A question that arises in developing any surface reaction lattice-gas simulation is how one relates the mean-field expressions for the rate of an elementary step of the reaction

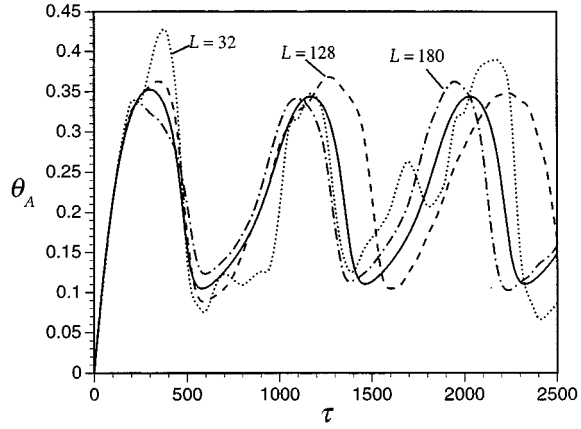

FIG. 5. Time series showing the effect of lattice size on lattice-gas simulations with no nearest-neighbor requirements for both dimer adsorption and reaction. The solid line represents the SA prediction. Other curves represent lattice-gas simulations on an $L \times L$ periodic square lattice, for various values of L as indicated. Parameter values used to construct the figure are $\beta=20.8$, $\alpha=1.6$, $\gamma=0.04$, $\lambda=0.36$, and $\eta=0.016$.

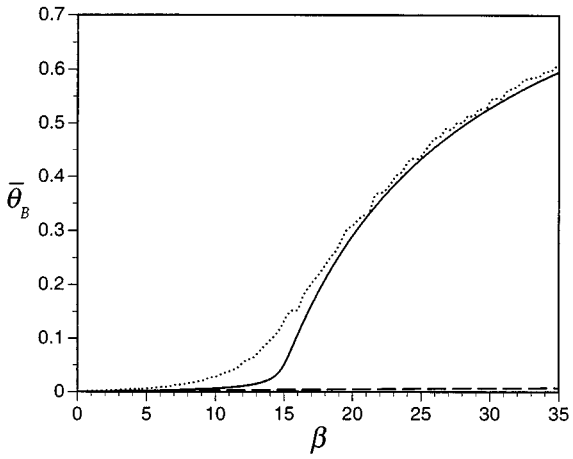

FIG. 6. Comparison of SA predictions (solid line) with lattice-gas simulations when the nearest-neighbor requirement is retained only for a reaction (dotted line) and when it is retained only for dimer adsorption (dashed line). Parameter values used to construct the figure are $\alpha=1.2$, $\gamma=0.04$, $\lambda=0.36$, and $\eta=0.016$.

mechanism to the rate at which a particular discrete event occurs in the lattice-gas simulation. This question has considerable relevance because it is desirable to compare the dynamic behavior of lattice-gas simulations with the predictions of mean-field rate equations.

The usual method for maintaining correspondence between the rate equations and the simulations involves (i) selecting sites at random and (ii) attempting the various elementary processes with the appropriate probabilities at the chosen sites. The algorithm implemented in this study reverses the above procedure. The rates of the elementary processes were first calculated by examining the state of the lattice. For example, the instantaneous rates of monomer and dimer adsorption were calculated as $\alpha\theta_V$ and $2\beta X_{VV}$, respectively. These rates were then used to select events with appropriate probabilities, and the selected events were executed at suitable randomly chosen sites. By requiring that one unit of Monte Carlo time (defined as N iterations of the algorithm, where N is the total number of lattice sites) correspond to one unit of dimensionless time τ, it was possible to execute events in the simulation randomly, but also in a manner that preserved the meanings of the dimensionless rate constants used in the mean-field formulations.

The simulation was first tested by ignoring spatial correlations on the lattice. This was accomplished by eliminating the nearest-neighbor (NN) requirements for dimer adsorption and monomer-dimer reaction, thereby resulting in a stochastic implementation of the SA equations. Representative simulations are presented in Fig. 5, which shows the effects of lattice size on time series predictions for a case in which the SA yields limit cycle oscillations. Notice that as the lattice size (and therefore the statistical base) increases, statistical fluctuations decrease and the lattice-gas simulations approach the mean-field SA predictions. These findings agree with the expectation that deviations from the mean-field site approximation are caused by multisite processes and, for finite systems, statistical fluctuations.

Because multisite processes are responsible for the breakdown of the site approximation, it is of interest to determine the relative importance of each such process in producing these deviations. This can be accomplished by eliminating the NN requirement for either dimer adsorption or reaction, while retaining the requirement for the other process. Predictions from such simulations are shown in Fig. 6 and they illustrate the significantly different impacts that NN requirements for dimer adsorption and reaction have on the overall behavior. In particular, when the NN requirement for dimer adsorption is neglected (this is similar to the random dimer adsorption model introduced by Tammaro and Evans [16]), the resulting reaction-adsorption isotherm closely approximates the SA prediction. In contrast, elimination of the NN requirement for reaction leads to large discrepancies between the lattice-gas simulations and the mean-field results. Most noticeably, the lattice-gas simulations predict a much lower steady-state surface coverage by the adsorbed dimer. The reason for this large deviation is that NN reactions are a source of NN vacancies; the presence of the latter is necessary for dimer adsorption to proceed. In the present case the removal of the NN requirement for reaction results in the production of far fewer vacant pairs suitable for dimer adsorption. These observations suggest that (for the parameter set studied) the NN requirement for dimer adsorption is the major cause of the breakdown of the site approximation.

When the NN requirements for both dimer adsorption and reaction are retained, behavior similar to that exhibited by the pair approximation is found. For example, Fig. 7 illustrates the effects of allowing adspecies to hop to nearest-neighbor vacant sites, for the case $d_A=d_B=d_C$. The resulting reaction-adsorption isotherms are nearly identical to those predicted by the pair equations for the same parameter set (Fig. 2). However, because the lattice-gas simulations are susceptible to random fluctuations, it can be difficult to detect the onset of kinetic oscillations. Therefore, three curves for each value of the dimensionless hopping constant were plotted in Fig. 7. The central curves (broken lines) represent

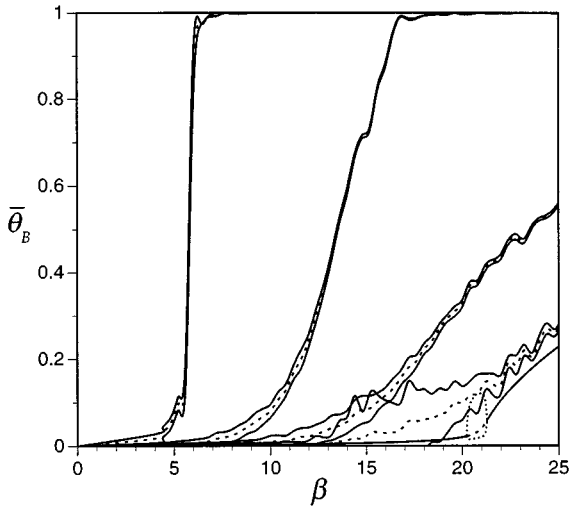

FIG. 7. Reaction-adsorption isotherms showing the convergence of the lattice-gas simulations and the site approximation when all adspecies have identical hopping rate constants. The curves from left to right show lattice-gas results for $d_i/k_3=0,1,4,16$. The last curve shows the SA prediction. For each lattice-gas simulation, three lines are plotted. The central line (dashed) represents the time-averaged B coverage at steady state; these are bracketed by solid lines that are the time-averaged coverage $\pm$ the variance divided by the mean. Parameter values used to construct the figure are the same as for Fig. 2.

the time-averaged steady-state B coverage; each of these is bracketed by two solid curves that represent the time-averaged coverage plus (minus) the variance divided by the mean. Figure 7 clearly shows that large excursions from the time-averaged coverage (indicative of kinetic oscillations) do not emerge until d_i/k_3 is increased to ≈ 16, which is similar to the value of $d_i/k_3 \approx 10$ found from the pair approximation. Also, notice that the discontinuous dimer poisoning transition predicted by the pair equations for low hop rates is also observed in the lattice-gas simulations.

MINIMUM DIFFUSION COEFFICIENT FOR OSCILLATIONS

The adsorbate hopping mechanism employed in the lattice-gas simulations and in the pair approximation can be related to Fickian diffusion by either solving the problem of random walk or by following the analysis of Kutner [17]. The hopping constant d (assumed to be identical for all species) is directly proportional to the diffusivity D through the relation

$$d=\frac{D}{l^2}, \tag{7}$$

where l is the lattice constant. If we take $d/k_3 \approx 10$ (the approximate value for oscillatory behavior to be supported by the pair equations and lattice-gas simulations), then one expects that the minimum value of the macroscopic surface diffusion coefficient required to observe oscillations for this reaction model is given by

$$D \approx 10 k_3 l^2. \tag{8}$$

SUMMARY AND DISCUSSION

Three approaches have been employed to model a simple Langmuir-Hinshelwood reaction: (i) traditional mean-field site approximation rate equations, (ii) mean-field pair approximation rate equations, and (iii) lattice-gas simulations. The oscillatory solutions predicted by the mean-field SA rate equations are not robust with respect to spatial correlations; both the PA equations (which account for nearest-neighbor correlations) and the lattice-gas simulations (which account for correlations on all length scales) fail to duplicate the periodic solutions.

The crossover behavior between the latter approaches and the SA was studied by incorporating an adspecies hopping mechanism. The structure of the kinetics for these intermediate degrees of ''mixing'' on the surface depends sensitively upon both the relative and absolute mobilities of the adspecies. Specifically, when all adspecies are mobile, the predictions of the SA, including kinetic oscillations, can be recovered when the ratio of the hopping constant to the reaction rate constant approximately satisfies $d/k_3 > 10$. However, if only one adspecies has significant surface mobility, the SA solutions cannot be approached even as the ratio of the hopping constant to the reaction rate constant becomes very large. These findings suggest that the use of SA rate equations to model real surface reaction schemes may not be appropriate when one or more species is strongly adsorbed.

A comparison of the PA and lattice-gas results reveals little qualitative difference (apart from the random fluctuations inherent in the lattice-gas simulation) and only small numerical discrepancies between their predictions. This apparent similarity is a consequence of the fact that the reaction mechanism involves only single- and dual-site processes; one might expect that greater disparity between the PA and the lattice-gas simulations would be observed for reaction mechanisms with processes involving three or more neighboring sites.

Finally, we note that the destruction of oscillatory behavior with the introduction of spatial correlations in the present model contrasts with analogous studies of predator-prey kinetics. In particular, Satulovsky and Tomé have shown that the breakdown of the mean-field approximation can lead to the introduction of periodic behavior in a system that would otherwise only display fixed-point solutions [18]. This implies that the consequences of introducing spatial correlations in surface reaction kinetics may depend strongly on the details of the reaction mechanism.

ACKNOWLEDGMENT

The authors thank Professor James Evans at Iowa State University for helpful discussions.

APPENDIX: GENERALIZED DIMENSIONLESS PAIR APPROXIMATION EQUATIONS

$$\frac{dX_{AV}}{dt}=2\alpha X_{VV}+2\gamma X_{AA}+\eta X_{AC}+\frac{3X_{AB}X_{AA}}{\theta_A}+\frac{3X_{AB}^2}{2\theta_B}-X_{AV}\left(\alpha+\lambda+\gamma+\frac{3\beta X_{VV}}{2\theta_V}+\frac{3X_{AB}}{2\theta_A}\right)+\frac{3\sigma_A X_{AV}}{2}\times\left(\frac{2X_{AA}}{\theta_A}+\frac{2X_{VV}}{\theta_V}-\frac{X_{AV}}{\theta_A}-\frac{X_{AV}}{\theta_V}\right)+\frac{3\sigma_B X_{BV}}{2}\times\left(\frac{X_{AB}}{\theta_B}-\frac{X_{AB}}{\theta_V}\right)+\frac{3\sigma_C X_{CV}}{2}\left(\frac{X_{AC}}{\theta_C}-\frac{X_{AV}}{\theta_V}\right), \quad \text{(A1)}$$

$$\frac{dX_{AA}}{dt}=\alpha X_{AV}-2\gamma X_{AA}-\frac{3X_{AB}X_{AA}}{\theta_A}+\frac{3\sigma_A X_{AV}}{2}\left(\frac{X_{AV}}{\theta_V}-\frac{2X_{AA}}{\theta_A}\right), \quad \text{(A2)}$$

$$\frac{dX_{AB}}{dt}=\alpha X_{BV}-(\gamma+1)X_{AB}+\frac{3\beta X_{AV}X_{VV}}{2\theta_V}-\frac{3X_{AB}^2}{2}\left(\frac{1}{\theta_A}+\frac{1}{\theta_B}\right)+\frac{3\sigma_A X_{AV}}{2}\left(\frac{X_{BV}}{\theta_V}-\frac{X_{AB}}{\theta_A}\right)+\frac{3\sigma_B X_{BV}}{2}\left(\frac{X_{AV}}{\theta_V}-\frac{X_{AB}}{\theta_B}\right), \quad \text{(A3)}$$

$$\frac{dX_{AC}}{dt}=\alpha X_{CV}+\lambda X_{AV}-(\gamma+\eta)X_{AC}-\frac{3X_{AB}X_{AC}}{2\theta_A}+\frac{3\sigma_A X_{AV}}{2}\left(\frac{X_{CV}}{\theta_V}-\frac{X_{AC}}{\theta_A}\right)+\frac{3\sigma_C X_{CV}}{2}\left(\frac{X_{AV}}{\theta_V}-\frac{X_{AC}}{\theta_C}\right), \quad \text{(A4)}$$

$$\frac{dX_{BV}}{dt}=\gamma X_{AB}+\eta X_{BC}-(\alpha+\lambda)X_{BV}+\frac{3X_{AB}^2}{2\theta_A}+\frac{3\beta X_{VV}}{2\theta_V}(2X_{VV}-X_{BV})+\frac{3X_{AB}}{2\theta_B}(2X_{BB}-X_{BV})+\frac{3\sigma_A X_{AV}}{2}\left(\frac{X_{AB}}{\theta_A}-\frac{X_{BV}}{\theta_V}\right)+\frac{3\sigma_B X_{BV}}{2}\left(\frac{2X_{BB}}{\theta_B}+\frac{2X_{VV}}{\theta_V}-\frac{X_{BV}}{\theta_B}-\frac{X_{BV}}{\theta_V}\right)+\frac{3\sigma_C X_{CV}}{2}\left(\frac{X_{BC}}{\theta_C}-\frac{X_{BV}}{\theta_V}\right), \quad \text{(A5)}$$

$$\frac{dX_{BB}}{dt}=\tfrac{1}{2}\beta X_{VV}+\frac{3\beta X_{VV}X_{BV}}{2\theta_V}-\frac{3X_{AB}X_{BB}}{\theta_B}+\frac{3\sigma_B X_{BV}}{2}\left(\frac{X_{BV}}{\theta_V}-\frac{2X_{BB}}{\theta_B}\right), \quad \text{(A6)}$$

$$\frac{dX_{BC}}{dt}=\lambda X_{BV}-\eta X_{BC}+\frac{3\beta X_{VV}X_{CV}}{2\theta_V}-\frac{3X_{AB}X_{BC}}{2\theta_B}+\frac{3\sigma_B X_{BV}}{2}\left(\frac{X_{CV}}{\theta_V}-\frac{X_{BC}}{\theta_B}\right)+\frac{3\sigma_C X_{CV}}{2}\left(\frac{X_{BV}}{\theta_V}-\frac{X_{BC}}{\theta_C}\right), \quad \text{(A7)}$$

$$\frac{dX_{CV}}{dt}=2\lambda X_{VV}+2\eta X_{CC}+\gamma X_{AC}-(\alpha+\lambda+\eta)X_{CV}-\frac{3\beta X_{VV}X_{CV}}{2\theta_V}+\frac{3X_{AB}}{2}\left(\frac{X_{BC}}{\theta_B}-\frac{X_{AC}}{\theta_A}\right)+\frac{3\sigma_A X_{AV}}{2}\left(\frac{X_{AC}}{\theta_A}-\frac{X_{CV}}{\theta_V}\right)+\frac{3\sigma_B X_{BV}}{2}\left(\frac{X_{BC}}{\theta_B}-\frac{X_{CV}}{\theta_V}\right)+\frac{3\sigma_C X_{CV}}{2}\left(\frac{2X_{CC}}{\theta_C}+\frac{2X_{VV}}{\theta_V}-\frac{X_{CV}}{\theta_C}-\frac{X_{CV}}{\theta_V}\right), \quad \text{(A8)}$$

$$\frac{dX_{CC}}{dt}=\lambda X_{CV}-2\eta X_{CC}+\frac{3\sigma_C X_{CV}}{2}\left(\frac{X_{CV}}{\theta_V}-\frac{2X_{CC}}{\theta_C}\right), \quad \text{(A9)}$$

$$\sum X_{ij}=1. \quad \text{(A10)}$$

The dimensionless parameters in Eqs. (A1)–(A9) are defined as $\alpha=k_1p_A/k_3$, $\beta=k_2p_{B_2}/k_3$, $\gamma=k_{-1}/k_3$, $\lambda=k_4p_C/k_3$, $\eta=k_{-4}/k_3$, and $\sigma_i=d_i/k_3$.

[1] Ronald Dickman, Phys. Rev. A **34**, 4246 (1986).
[2] Martine Dumont, P. Dufour, B. Sente, and R. Dragonnier, J. Catal. **122**, 95 (1990).
[3] J. W. Evans and M. S. Miesch, Surf. Sci. **245**, 401 (1991).
[4] M. Ehsasi, M. Matloch, O. Frank, and J. H. Block, J. Chem. Phys. **91**, 4949 (1989).
[5] R. M. Ziff, E. Gulari, and Y. Barshad, Phys. Rev. Lett. **56**, 2553 (1986).
[6] J. W. Evans, J. Chem. Phys. **97**, 572 (1992).
[7] H. P. Kaukonen and R. M. Nieminen, J. Chem. Phys. **91**, 4380 (1989).
[8] Iwan Jensen and Hans C. Fogedby, Phys. Rev. A **42**, 1969 (1990).
[9] J. Mai, V. N. Kuzovkov, and W. von Niessen, Physica A **203**, 298 (1994).
[10] J. W. Evans and T. R. Ray, Phys. Rev. E **50**, 4302 (1994).
[11] M. Tammaro, M. Sabella, and J. W. Evans, J. Chem. Phys. **103**, 10 277 (1995).
[12] Ru-Sheng Li and W. Horsthemke, J. Chem. Phys. **95**, 5785 (1991).
[13] M. C. Lemos, J. J. Luque, and F. Jimenez-Morales, Phys. Rev. E **51**, 5360 (1995).
[14] G. Eigenberger, Chem. Eng. Sci. **33**, 1263 (1978).
[15] E. Doedel and X. Wang, Auto94: *Software for Continuation and Bifurcation Problems in Ordinary Differential Equations*, Applied Mathematics Department, California Institute of Technology, 1994.
[16] M. Tammaro and J. W. Evans, Phys. Rev. E **52**, 2310 (1995).
[17] R. Kutner, Phys. Lett. **81A**, 239 (1981).
[18] J. E. Satulovsky and T. Tomé, Phys. Rev. E **49**, 5073 (1994).